Systematic study of neutron capture including the compound, pre-equilibrium, and direct mechanisms

Y. Xu and S. Goriely
Institut d'Astronomie et d'Astrophysique, C.P. 226, Université Libre de Bruxelles, bd. du Triomphe, B-1050 Brussels, Belgium

A. J. Koning
Nuclear Research and Consultancy Group, P.O. Box 25, NL-1755 ZG Petten, The Netherlands

S. Hilaire
CEA, DAM, DIF, F-91297 Arpajon, France

(Received 3 April 2014; revised manuscript received 23 July 2014; published 7 August 2014)

The neutron capture reaction is investigated. The three major reaction mechanisms, namely, compound-nucleus capture (CNC), pre-equilibrium capture (PEC), and direct capture (DIC), are considered on the basis of the Hauser–Feshbach model, the exciton model, and potential model, respectively. The three mechanisms are treated simultaneously and consistently, i.e, they are obtained on the basis of the same nuclear ingredients, such as the optical potential and nuclear-level densities. In this framework, the three components are calculated on the same footing and represent partial fluxes of the same total reaction cross section. The total neutron-capture cross sections and astrophysical reaction rates are calculated within the updated modern reaction code TALYS for about 8000 nuclei with $8 \leqslant Z \leqslant 110$ lying between the proton and neutron drip lines. The nuclear-structure ingredients involved in the calculation are determined from experimental data whenever available and, if not, from global microscopic nuclear models. For the targets with mass number $A > 26$, a fair agreement between the computed total-capture cross sections and experimental data is found but, for the lightest nuclei, only the predicted DIC cross sections reproduce the experimental results satisfactorily. Significant and even dominant contribution to the total reaction rate comes from the DIC component for neutron-rich nuclei, especially in the $Z = 50$–70 region. The impact of the newly determined reaction rates on the r process abundances resulting from the ejection of matter in neutrino-driven winds or the decompression of neutron star matter is investigated.

DOI: 10.1103/PhysRevC.90.024604 PACS number(s): 24.10.−i, 24.50.+g, 25.60.Tv, 26.30.−k

I. INTRODUCTION

Nuclear reactions of astrophysical interest often concern unstable or even exotic species for which no experimental data exist. Although significant efforts have been devoted in the past decades, experimental information only covers a minute fraction of the entire data set required for nuclear astrophysics. Moreover, the energy range for which experimental data is available is restricted to the small range that can be studied by present experimental setups. For all unknown cases, only theoretical predictions can fill the gaps. One of these specific examples concerns the rapid neutron-capture process (r process) called for to explain the origin of about half of the elements heavier than iron observed in nature (for a review, see Ref. [1]). The r process is believed to take place in environments characterized by high neutron densities, such that successive neutron captures can proceed into neutron-rich regions well off the β-stability valley. It involves a large number (typically five thousand) of unstable nuclei for which many different properties have to be determined and cannot be obtained experimentally. One such fundamental property concerns the radiative neutron-capture reaction.

Radiative neutron capture is traditionally estimated within the statistical Hauser–Feshbach model [2,3]. The model makes the fundamental assumption that the capture process takes place with the intermediary formation of a compound nucleus in thermodynamic equilibrium. The energy of the incident particle is then shared more or less uniformly by all the nucleons before releasing the energy by particle emission or γ deexcitation. In the Hauser–Feshbach approach, the formation of a compound nucleus is usually justified by assuming that the nuclear level density (NLD) in compound nuclei at the projectile incident energy is large enough to ensure an average statistical continuum superposition of available resonances [4]. For medium- and heavy-mass nuclei lying within the valley of stability, the compound-nucleus capture (CNC) at energies of astrophysical interest is known to be the dominant reaction mechanism [1,3,4].

However, when the number of available states in a compound nucleus is relatively small, the capture reaction is possibly dominated by direct electromagnetic transitions to a bound final state rather than through a compound-nucleus intermediary. This direct capture (DIC) proceeds via the excitation of only a few degrees of freedom on a much shorter time scale, reflecting the time taken by the projectile to travel across the target. This mechanism can be satisfactorily described with the perturbative approach known as the potential model [5–9]. It is now well accepted that the DIC process is important and often dominant at the very low energies of astrophysical interest for light or exotic nuclei systems for which few or even no resonant states are available [10–15].

In between these two extreme CNC and DIC processes lies the so-called pre-equilibrium capture (PEC) characteristic of high-energy collisions where particles can be emitted after the

first direct interaction and before the statistical equilibrium can be reached. The PEC process is responsible for the observed increase of the radiative neutron capture cross section for stable nuclei at incident energies typically around 10 MeV. However, for exotic neutron-rich nuclei with low neutron separation energies and low NLD, the PEC process starts to affect the neutron channel already at a few hundred keV because of the difficulty to achieve a full equilibrium for such nuclei. It has been shown [16] that the exciton model can describe the PEC process in a satisfactory way.

The CNC, PEC, and DIC contributions to nuclear reactions are known not to be mutually exclusive. All mechanisms may contribute to the radiative capture of a neutron. For this reason, the total cross section is usually taken as the simple sum of these contributions, neglecting all possible interferences between them. However, the three contributions are often calculated on the basis of different nuclear ingredients [7,9]; in particular, different optical potentials and level densities. In this case, each contribution is characterized by a different total reaction cross section and adding them up is inconsistent. It is indeed of prime importance when comparing the contribution of each of these capture processes that the treatment be based on the same footing with the same nuclear ingredients.

In the present paper, we present new systematic calculations of the neutron-capture cross sections and reaction rates for which the CNC, PEC, and DIC contributions are included simultaneously and consistently. In particular, we emphasize that (i) all calculations are performed with the unique updated reaction code TALYS [17–19] in which the potential model for DIC reaction has been introduced, and (ii) the same set of nuclear-structure ingredients are employed to compute all the three contributions. In Sec. II, the Hauser–Feshbach model for the CNC contribution, the exciton model for the PEC contribution, and the potential model for the DIC contribution are described. Detailed nuclear-structure ingredients used in these models are provided in Sec. III; this includes the nuclear ground-state properties, the neutron-nucleus interaction potential, the γ-ray strength function, as well as the excitation spectrum deduced from the discrete experimental levels and the NLD. These new developments of the TALYS code are briefly introduced in Sec. IV. Results are discussed in Sec. V, including the comparison between model predictions and experimental data, the prediction of the total neutron-capture reaction rates for about 8000 nuclei with $8 \leqslant Z \leqslant 110$ lying between the proton and neutron drip lines, and the explicit analysis of CNC, PEC, and DIC contributions to the total neutron-capture reaction rates. As an illustration of the impact of the newly derived radiative neutron-capture rates, r-process nucleosynthesis simulations are performed in Sec. VI. Finally, we summarize the results in Sec. VII.

II. REACTION MODELS

A. Hauser–Feshbach model for compound-nucleus capture

The Hauser–Feshbach model relies on the fundamental Bohr hypothesis that the capture process occurs by means of the intermediary formation of a compound nucleus that can reach a state of thermodynamic equilibrium. It is valid if the formation and decay of the compound nucleus are independent [2]. The formation of a compound nucleus is known to be fulfilled if the NLD in the compound nucleus at the excitation energy corresponding to the projectile incident energy is sufficiently high.

Provided the reaction $A + n = B + \gamma$ represents the neutron capture onto the nucleus A leaving the residual nucleus B and the photon, the corresponding binary cross section by the CNC can be written as

$$\sigma^{\mathrm{CNC}}(E) = \sum_{x=0}^{A} \sum_{x=0}^{B} \sigma^{\mathrm{CNC}}_{A^x+n\to B^x+\gamma}(E). \tag{1}$$

The summation $\sum_{x=0}^{A}$ and $\sum_{x=0}^{B}$, where the energy-level scheme is represented by the xth excited state ($x = 0$ is the ground state), covers all the possible states (ground and excitation states) of the target A and residual nucleus B. Each state is characterized by a spin S_A^x, a parity π_A^x, and an excitation energy E_A^x for the target A (and similarly for the residual nucleus B).

The expression for the cross section $\sigma^{\mathrm{CNC}}_{A^x+n\to B^x+\gamma}(E)$ is given by (see, e.g., Ref. [3])

$$\begin{aligned}
&\sigma^{\mathrm{CNC}}_{A^x+n\to B^x+\gamma}(E) \\
&= \frac{\pi}{k^2} \sum_{J=\mathrm{mod}(S_A^x+S_n,1)}^{l_{\max}+S_A^x+S_n} \sum_{\Pi=-1}^{1} \frac{2J+1}{(2S_A^x+1)(2S_n+1)} \\
&\times \sum_{J_n=|J-S_A^x|}^{J+S_A^x} \sum_{l_i=|J_n-S_n|}^{J_n+S_n} \sum_{\lambda=|J-S_B^x|}^{J+S_B^x} \sum_{l_f=|\lambda-S_\gamma|}^{\lambda+S_\gamma} \\
&\times \delta^{\pi}_{C_n} \delta^{\pi}_{C_\gamma} \frac{\langle T^J_{C_n,l_i,J_n}(E)\rangle \langle T^J_{C_\gamma,l_f,\lambda}(E_\gamma)\rangle}{\sum_{Clj} \delta^{\pi}_{C} \langle T^J_{Clj}(E_C)\rangle} W^J_{C_n l_i J_n C_\gamma l_f \lambda},
\end{aligned} \tag{2}$$

where k is the wave number of the relative motion, E is the incident energy of the neutron as the projectile, E_γ is the energy of the emitted photon, $l_{\max}$ is the maximum value of the relative orbital momentum l_i of target A and neutron n, S_n is the spin of the neutron, J_n is its total angular momentum, S_γ is the photon spin; l_f is the relative orbital momentum of the residual nucleus B and the photon, λ is the multipolarity of the photon (total angular momentum of photon) coupled by S_γ and l_f, J and Π are the total angular momentum and parity of the compound nucleus, respectively, C_n is the channel label of the initial system ($n + A^x$) designated by $C_n = (n, S_n, E, E_A^x, S_A^x, \pi_A^x)$, C_γ is the channel label of the final system ($\gamma + B^x$) designated by $C_\gamma = (\gamma, S_\gamma, E_\gamma, E_B^x, S_B^x, \pi_B^x)$, $\delta^{\pi}_{C_n} = 1$ if $\pi_A^x \pi_n (-1)^{l_i} = \Pi$ and 0 otherwise, $\delta^{\pi}_{C_\gamma} = 1$ if $\pi_B^x \pi_\gamma (-1)^{l_f} = \Pi$ and 0 otherwise, π_n is the parity of the neutron, π_γ is the parity of the photon, T is the transmission coefficient, $\sum_{Clj} \delta^{\pi}_{C} \langle T^J_{Clj}(E_C)\rangle$ is the sum of the transmission coefficient T for all possible decay channels C of the compound nucleus, and W is the width fluctuation correction factor for which different approximate expressions are described and discussed in Ref. [20].

The transmission coefficient T is estimated for each level with known energy, spin, and parity.

If the excitation energy E^x, which is implicit in the definition of channel C, corresponds to a state in the continuum, an effective transmission coefficient is defined for an excitation-energy bin of width ΔE by the integral

$$\left\langle T^J_{Clj}\left(E_C\right)\right\rangle = \int_{E^x-\Delta E/2}^{E^x+\Delta E/2} \rho\left(E,J,\Pi\right) T^J_{Clj}\left(E_C\right) dE \qquad (3)$$

over the NLD $\rho(E,J,\Pi)$. Note that the various transmission coefficients T, corresponding to the reaction channels open, depend on different nuclear ingredients. In particular, the transmission coefficient for particle emission is determined by the optical potentials between the two interacting particles, while the photon transmission coefficient relies on the γ-ray strength function. Detailed nuclear-structure ingredients that are used to determine the transmission coefficient T are described in Sec. III.

B. Exciton model for pre-equilibrium capture

For increasing energy or nuclei for which the CNC does not have time to reach thermodynamic equilibrium, PEC or DIC processes may become significant. PEC can occur after the first stage of the reaction but long before statistical equilibrium of the compound nucleus is reached.

One of the most widely used model to describe the PEC mechanism is the (one- or two-component) exciton model [16], in which the nuclear state is characterized at any moment during the reaction by the total energy and the total number of particles above and holes below the Fermi surface. Particles (p) and holes (h) are referred to as excitons. Furthermore, it is assumed that all possible ways of sharing the excitation energy between different particle-hole configurations at the same exciton number $n = p + h$ have an equal *a-priori* probability. The basic starting point of the exciton model is a time-dependent master equation, which describes the probability of transitions to more and less complex p-h states as well as transitions to the continuum (emission). Ref. [16] provides the complete formalism of the exciton model as included in the TALYS reaction code.

The relative contribution between the CNC and PEC cross sections has been studied in Ref. [3] and will consequently not be repeated in the present study.

C. Potential model for direct capture

The potential model, as a perturbative approach, is employed to study the neutron DIC reaction describing the transition from the initial scattering state $A + n$ directly to the final nucleus B with accompanying γ-ray emission. The allowed electric-dipole ($E1$), electric-quadrupole ($E2$) and magnetic-dipole ($M1$) transitions to the ground state as well as all possible excited states in the final nucleus are taken into account. Note that we consider transitions to all possible energy levels, including not only the discrete levels but also the continuum described by a combinatorial model of NLD, as detailed in Refs. [7,9].

The neutron DIC cross section for $A(n,\gamma)B$ can be expressed as [7]

$$\sigma^{\mathrm{DIC}}\left(E\right) = \sum_{x=0}^{E^x_B} S^x_F \sigma^{\mathrm{DIC}}_{A+n\to B^x+\gamma}\left(E\right) + \left\langle S_F\right\rangle \int_{E^x_B}^{S_n} \sum_{S^x_B,\pi^x_B} \rho\left(E,S^x_B,\pi^x_B\right)\sigma^{\mathrm{DIC}}_{A+n\to B^x+\gamma}\left(E\right) dE. \qquad (4)$$

Below E^x_B, the sum runs over all available discrete final states (i.e., the experimentally known energy levels) in the residual nucleus B. S^x_F is the spectroscopic factor describing the overlap between the antisymmetrized wave function of the initial system $A + n$ and the final state B^x. Above E^x_B, the summation is replaced by a continuous integration over a spin- and parity-dependent NLD $[\rho(E,S^x_B,\pi^x_B)]$ and the spectroscopic factor by an average quantity $\langle S_F\rangle$.

The potential model calculates the transition matrix element between the initial and the final states by sandwiching the electromagnetic operators in the long-wavelength limit. It is usually enough to consider the $E1$, $E2$, and $M1$ transitions [9]. For a transition from the initial $A + n$ system to the final state $B^x + \gamma$, the partial cross section $\sigma^{\mathrm{DIC}}_{A+n\to B^x+\gamma}(E)$ can be written as

$$\sigma^{\mathrm{DIC}}_{A+n\to B^x+\gamma}\left(E\right) = \frac{2S^x_B+1}{Ek\left(2S_A+1\right)\left(2S_n+1\right)} \times \sum_{I_f,J_i,l_i,I_i} \left\{\frac{2}{9}k^3_\gamma\left(|M_{E1}|^2+|M_{M1}|^2\right) + \frac{1}{150}k^5_\gamma|M_{E2}|^2\right\}. \qquad (5)$$

In Eq. (5), S^x_B, S_A, and S_n are the spin of the nucleus B^x, A, and the neutron, respectively, and k_γ is the wave number of the emitted photon. The summations run over the channel spin I_i, orbital angular momentum l_i, and total angular momentum J_i of the initial system $A + n$, and over the channel spin I_f of the final state. The matrix elements consist of two components, the radial moments ($\mathcal{M}_{E1}$, $\mathcal{M}_{E2}$, $\mathcal{M}_{M1}$) and, if any, the internal moments of the nucleus A [$\mathcal{M}^{\mathrm{int}}_{M1}(A)$, $\mathcal{M}^{\mathrm{int}}_{E2}(A)$] and neutron [$\mathcal{M}^{\mathrm{int}}_{M1}(n)$, $\mathcal{M}^{\mathrm{int}}_{E2}(n)$], which are given by

$$\begin{aligned} M_{E1} &= \mathcal{M}_{E1}, \\ M_{M1} &= \mathcal{M}_{M1} + \mathcal{M}^{\mathrm{int}}_{M1}\left(A\right) + \mathcal{M}^{\mathrm{int}}_{M1}\left(n\right) \\ M_{E2} &= \mathcal{M}_{E2} + \mathcal{M}^{\mathrm{int}}_{E2}\left(A\right) + \mathcal{M}^{\mathrm{int}}_{E2}\left(n\right). \end{aligned} \qquad (6)$$

The complete formula of the matrix elements can be found in Ref. [9].

Nuclear potentials $V(E,r)$ are employed to solve the radial part of the two-body Schrödinger equation

$$\left[\frac{d^2}{dr^2} - \frac{l\left(l+1\right)}{r^2} + \frac{2\mu}{\hbar^2}\left\{E - V\left(E,r\right)\right\}\right]\psi = 0 \qquad (7)$$

in the relative coordinate r and to derive the radial wave functions $\psi = \phi_{nl}(r)$ for bound state B^x ($E < 0$) and $\psi = \chi_l(E,r)$ for initial scattering system $A + n$ ($E > 0$). In

Eq. (7), l is the relative orbital angular momentum, and $\mu = m_A m_n/(m_A + m_n)$ is the reduced mass.

For the scattering system $A + n$ [$E = \hbar^2 k^2/(2\mu)$ with the wave number k and the reduced mass μ], the radial wave functions $\chi_l(k,r)$ behave asymptotically at large distances as

$$\chi_l(k,r) \longrightarrow e^{i\delta_l}\left[\cos(\delta_l)\, kr J_l(kr) - \sin(\delta_l)\, kr Y_l(kr)\right]. \quad (8)$$

In Eq. (8), δ_l is the phase shift of elastic scattering by the nuclear potential, and $J_l(kr)$ and $Y_l(kr)$ are the Bessel functions of first and second kinds, respectively.

For bound state B^x, the radial wave function $\phi_{nl}(r)$ must vanish at infinity and be normalized as

$$\int_0^\infty |\phi_{nl}(r)|^2 dr = 1, \quad (9)$$

where n stands for the radial quantum number. More details on the adopted DIC potential model can be found in Refs. [7,9].

Finally, note that the semidirect capture component is approximated here in terms of pre-equilibrium γ emission and is therefore not consistently described with respect to the direct mechanism. As shown in Ref. [14], the semidirect component gives a negligible contribution to the low-energy cross section, and hence to the astrophysical reaction rates.

III. NUCLEAR INGREDIENTS

The nuclear inputs required for calculations can be extracted from basic nuclear-structure properties. Whenever available, the nuclear ingredients are taken from experiment. If not, global models, as described below, are considered. For a reliable prediction, such models need to be as microscopic as possible, especially when dealing with exotic neutron-rich nuclei for which extrapolation is required. Such a microscopic description provided by physically sound theories based on first principles likely renders extrapolations away from experimentally known energy or mass regions more reliable than predictions derived from more-or-less parametric phenomenological approaches of various types and levels of sophistication.

A. Nuclear mass, electromagnetic multipole moment, and spectroscopic factor

Nuclear masses are taken from the 2012 Atomic Mass Evaluation [21] whenever available. When not available, masses are predicted by the Hartree–Fock–Bogoliubov (HFB) method based on the BSk21 Skyrme interaction, namely, the HFB-21 mass model [22].

The nuclear magnetic-dipole (μ_1) and electric-quadrupole (Q_2) moments appearing in the potential model calculation are taken from the experimental data compilation of Ref. [23]. When no data are available, the single-particle model is used for predicting the nuclear magnetic-dipole moment, while the nuclear deformations (β_2) obtained within the HFB-21 calculation [22,24] are used to estimate the electric-quadrupole moments.

For the spectroscopic factors, experimental results compiled in Ref. [25] are included for the discrete level contributions [Eq. (4)]. When no experimental data exists for experimentally known levels, an average value $\langle S_F \rangle = 0.347$ is adopted. This value corresponds to the average value from all the compiled experimental spectroscopic factors [25] for levels with allowed $E1$, $E2$ and $M1$ transitions. On the other hand, for theoretically determined levels, pure neutron 1 p 1 h excitations are considered here (see Sec. III D) for which an averaged spectroscopic factor $\langle S_F \rangle = 1$ is adopted [9].

B. γ-ray strength function

Large-scale derivations of the γ-ray strength function [26] have been conducted with the use of the HFB plus quasiparticle random phase approximation (QRPA) models [27]. The HFB + QRPA model is known to be an accurate tool to estimate the γ-ray strength function in both closed- and open-shell nuclei [26]. In the present calculation, the γ-ray strength functions obtained from the HFB + QRPA models based on the BSk7 Skyrme force are included in the Hauser–Feshbach model to compute the electromagnetic transmission coefficients.

C. Nuclear potential

The so-called Bruyères Jeukenne–Lejeune–Mahaux (JLMB) optical potential is adopted in the present calculations. It corresponds to the Bruyères-le-Châtel renormalization [28] of the Jeukenne–Lejeune-Mahaux potential [29]. The JLMB potential is a global semimicroscopic nucleon-nucleus spherical optical model potential adjusted on $A = 30$ to 240 nuclei and for energies ranging from 10 keV up to 200 MeV [28,30,31]. The JLMB potential was phenomenologically renormalized in Refs. [28,32] to improve the agreement between experimental and predicted observables for a large set of data.

The JLMB potential for a given nuclear matter density $\rho = \rho_n + \rho_p$ and asymmetry $\alpha = (\rho_n - \rho_p)/\rho$ reads

$$V(E,r) = \lambda_V(E)\left[V_0(E) + \lambda_{V1}(E)\,\alpha V_1(E)\right] + i\lambda_W(E)\left[W_0(E) + \lambda_{W1}(E)\,\alpha W_1(E)\right], \quad (10)$$

with E being the incident nucleon energy; $V_0(E)$, $V_1(E)$, $W_0(E)$, and $W_1(E)$ are the real isoscalar, real isovector, imaginary isoscalar, and imaginary isovector components, respectively; and $\lambda_V(E)$, $\lambda_{V1}(E)$, $\lambda_W(E)$, and $\lambda_{W1}(E)$ are their respective renormalization factors. The HFB-21 matter density (ρ_n and ρ_p) [22,24] are used to calculate the four components of the JLMB potential in Eq. (10) on the basis of the local density approximation applied to Brückner–Hartree–Fock calculation of nuclear matter [29,33]. The expressions for $\lambda_V(E)$, $\lambda_{V1}(E)$, $\lambda_W(E)$, and $\lambda_{W1}(E)$ can be found in Ref. [28].

For nuclear astrophysics applications, the JLMB nuclear potential has been extensively used in CNC and PEC calculations [3] as well as in DIC calculations [7,9]. In the present calculation, the very same JLMB potential is used consistently to estimate the total reaction cross section as well as the reaction flux feeding separately each of the three reaction components.

D. Nuclear level density and discrete-level scheme

As shown by Eqs. (3) and (4), the nuclear-level scheme is another crucial ingredient for the cross-section calculations.

For most nuclei, only few, if any, experimental levels are available. In this situation, we must resort to the use of a continuum level spectrum determined from a NLD model. Especially at low energies, a microscopic approach capable of estimating the nonstatistical spin and parity dependence of the NLD should be considered. The microscopic HFB plus a combinatorial approach has proven its capacity to reproduce not only the low-lying cumulative number of levels but also the neutron resonance spacings at the neutron-separation energy [61]. Based on this approach, the spin- and parity-dependent NLDs as well as the partial *ph* densities are estimated and used consistently in the different calculations of the CNC, PEC, and DIC contributions.

For the DIC calculations, it is well accepted that the predicted cross sections are in qualitatively good agreement with experimental results as long as all the details of the excitation spectrum are known experimentally [62,63]. For this reason, whenever available, the discrete experimental level schemes are taken from the RIPL-3 library [64] with their associated spectroscopic factor. Note that the main contribution to the DIC cross section often results from transitions to the ground state or to a small number of low-lying states, provided the selection rules allow for the considered electromagnetic transitions [7,9].

IV. TALYS

The present calculations are performed based on the updated version of TALYS [17–19], which is a software for the simulation of nuclear reactions. TALYS provides a complete description of all reaction channels and observables and, in particular, takes into account all types of direct, pre-equilibrium, and compound mechanisms to estimate the total reaction probability as well as the competition between the various open channels. Many state-of-the-art nuclear models to cover all the main reaction mechanisms encountered in light-particle-induced nuclear reactions are included, as presented in Sec. II. The code is optimized for incident projectile energies ranging from 1 keV to 200 MeV on target nuclei with mass numbers between 12 and 339. It includes photon, neutron, proton, deuteron, triton, ^{3}He, and α particles as both projectiles and ejectiles, and single-particle as well as multiparticle emissions and fission. TALYS was designed to calculate total and partial cross sections, residual- and isomer-production cross sections, discrete and continuum γ-ray-production cross sections, energy spectra, angular distributions, double-differential spectra, as well as recoil cross sections. For the nuclear ingredients used in the TALYS calculation, whenever available, all experimental information on nuclear masses, deformation, and spectra of low-lying states is considered; in particular, the RIPL-3 database [64]. If not, various local and global input models have been incorporated to represent the nuclear-structure properties, such as the optical potentials, NLD, and γ-ray strength functions. TALYS has been updated to estimate now the DIC contribution to the cross sections and reaction rates for all incident projectiles, following the model described in Sec. II C. It is now possible to estimate all the CNC, PEC, and DIC contributions consistently and simultaneously, making use of the same input physics.

V. RESULTS AND DISCUSSIONS

To test the neutron-capture reaction model, we compare in Fig. 1 our calculated total neutron-capture cross sections including CNC, PEC, and DIC mechanisms (solid lines) with the experimental data for nine neutron-capture reactions; namely, ^{27}Al, ^{37}Cl, ^{48}Ca, ^{61}Ni, ^{97}Mo, ^{122}Sn, ^{178}Lu, ^{208}Pb, and ^{232}Th. A rather good agreement is found, which confirms that the model is capable of predicting the neutron-capture cross section. For the nine targets, the DIC cross sections are also shown (dashed lines) in Fig. 1. As already found earlier, the DIC contribution becomes significant or even dominates the reaction mechanism for light species like ^{27}Al, ^{37}Cl, or ^{48}Ca; at least if no resonant states are clearly available.

Similarly in Fig. 2, we compare our calculated neutron-capture cross sections corresponding to all the CNC, PEC, and DIC mechanisms (solid lines) and the DIC mechanism only (dashed lines) with available experimental data for the four neutron-capture reactions on very light targets ^{16}O, ^{18}O, ^{22}Ne, and ^{26}Mg. Generally, it can be seen that the total (CNC + PEC + DIC) systematically overestimates the cross sections. Indeed, the CNC always assumes that the number of levels available to the incident nucleon in the compound nucleus is large enough and that their energy and width are randomly distributed within the contributing energy interval to ensure a continuum superposition of resonances. In this case, when none or only a small number of resonances are available, the CNC model is expected to overestimate the cross section. In contrast, the DIC model is seen in Fig. 2 to describe fairly well the experimental cross sections in such $A < 26$ cases.

The astrophysical Maxwellian-averaged reaction rate of neutron capture ($N_a\langle\sigma v\rangle$, where N_a is the Avogadro number and v the relative velocity between target and projectile) corresponding to the total (CNC + PEC + DIC), the CNC + PEC or only the CNC contributions are compared in Fig. 3 for the Sn and Pb isotopic chains at a temperature $T = 10^9$ K. At this temperature, the PEC contribution is seen to be small for all Sn and Pb isotopes. Only at larger temperatures $T \gtrsim 3 \times 10^9$ K can the PEC start to affect the total radiative capture rate [3]. For all the Sn and Pb stable and neutron-deficient isotopes the DIC contribution is also found to be negligible with respect to the CNC contribution. However, when considering more neutron-rich isotopes, the CNC contribution decreases while the DIC contribution remains significant and actually strongly dominates the capture mechanism in the exotic neutron-rich region. The DIC can lead to an increase of the radiative neutron-capture rate by one or two orders of magnitude for such nuclei at temperatures of the order of 10^9 K. The impact of the DIC contribution to the total rate also depends on the temperature. For open-shell nuclei, at increasing temperature, the CNC rate tends to decrease due to the opening of additional emission channels. In contrast, the DIC rate is less sensitive to the temperature, so that in general the DIC contribution tends to increase with increasing temperature, as illustrated in Fig. 4. However, in the case of the double closed-shell nucleus ^{132}Sn, even at low temperatures the CNC contribution is so small that the DIC already dominates the rate. The temperature dependence is inverted with respect to the open-shell Sn isotopes since, for ^{132}Sn, the CNC rate essentially increases with increasing temperatures.

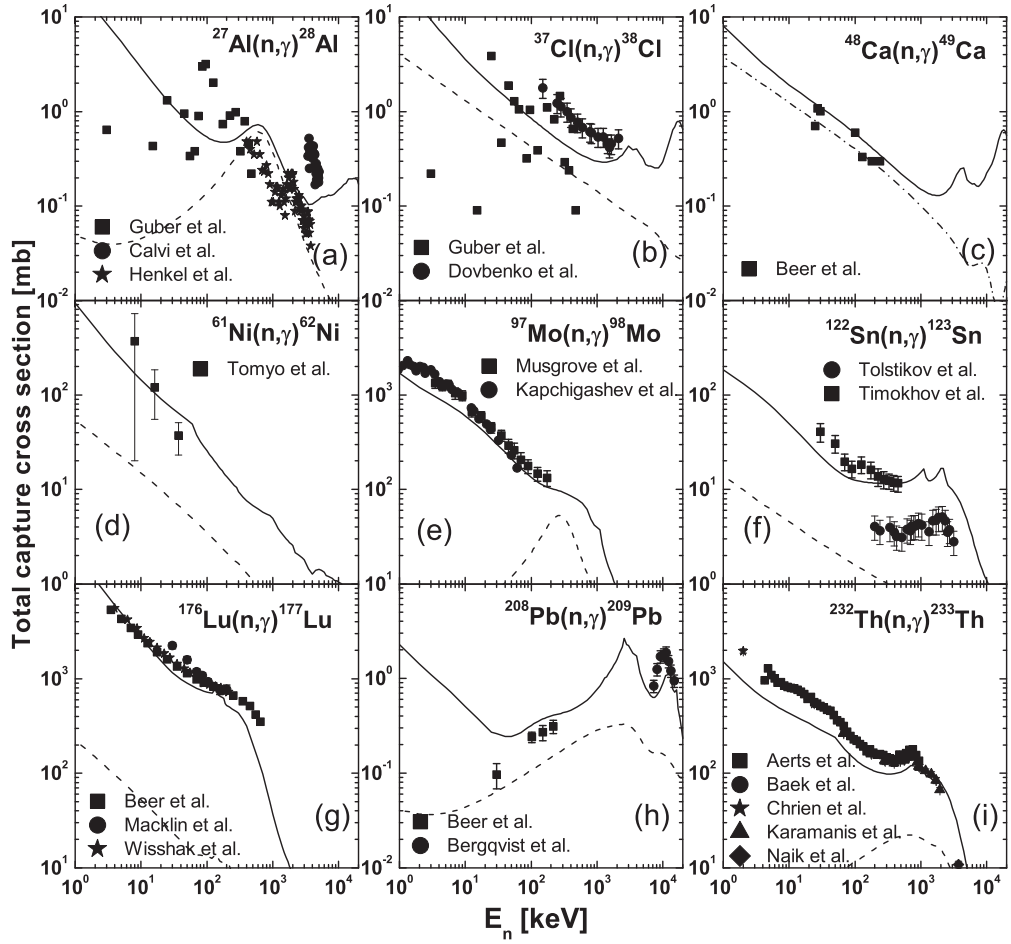

FIG. 1. Comparison of our calculated neutron-capture cross sections and the experimental data for nine nuclei. The solid lines correspond to the total (CNC + PEC + DIC) neutron-capture cross sections, while the dashed lines correspond to the DIC contribution only. Experimental data are taken from Refs. [34–36] for ^{27}Al(n,γ)^{28}Al, [34,37] for ^{37}Cl(n,γ)^{38}Cl, [13] for ^{48}Ca(n,γ)^{49}Ca, [38] for ^{61}Ni(n,γ)^{62}Ni, [39,40] for ^{97}Mo(n,γ)^{98}Mo, [41,42] for ^{122}Sn(n,γ)^{123}Sn, [43–45] for ^{176}Lu(n,γ)^{177}Lu, [46,47] for ^{208}Pb(n,γ)^{209}Pb, and [48–52] for ^{232}Th(n,γ)^{233}Th.

The reaction rates of astrophysics interest for neutron capture have been calculated for about 5800 nuclei with $8 \leqslant Z \leqslant 92$ lying between the $N = Z$ and neutron drip lines. Figure 5 shows the ratio between the total and the CNC reaction rates as a function of the neutron-separation energies. The DIC is seen to increase the radiative neutron-capture rate by a factor up to 10^4 for drip line nuclei. Figure 6 represents in the (N,Z) plane the same ratio and shows that most of the neutron-rich regions in between closed neutron shells are dominated by the DIC mechanism. However, for some neutron-rich nuclei, no allowed direct transitions may be found (due to selection rules), and the direct channel can consequently be inhibited [7].

VI. APPLICATION TO THE r-PROCESS NUCLEOSYNTHESIS

As an illustration of the impact of the newly derived radiative neutron-capture rates, r-process nucleosynthesis calculations have been performed. The impact of reaction rates on the r-process nucleosynthesis remains difficult to ascertain in the sense that their influence strongly depends on the adopted astrophysical scenario and most particularly of the temperature at which the r process takes place [1]. In particular, in the so-called cold r process, photodisintegration rates are slow and consequently no (n,γ)-(γ,n) equilibrium can be achieved. In this case, the neutron-capture rates directly influence the calculated abundances [1]. It should however be recalled here that, so far, all r-process calculations have made use of neutron-capture rates evaluated within the statistical model of Hauser–Feshbach and that the DIC component is never included in such calculations.

Despite a growing wealth of observational data (see, e.g., Ref. [65]) and increasingly better r-process models with new astrophysical or nuclear physics ingredients, the stellar production site(s) of r-process material has (have) not been identified yet. All proposed scenarios face serious problems. For this reason, we have considered here the two most popular r-process models nowadays, i.e, the ν-driven wind model in supernova explosions of massive stars [66–68] and the decompression of neutron star matter during the merging of binary neutron stars [69,70].

The nucleosynthesis is followed with a reaction network including all 5000 species from protons up to $Z = 110$ lying between the valley of β stability and the neutron drip line. All

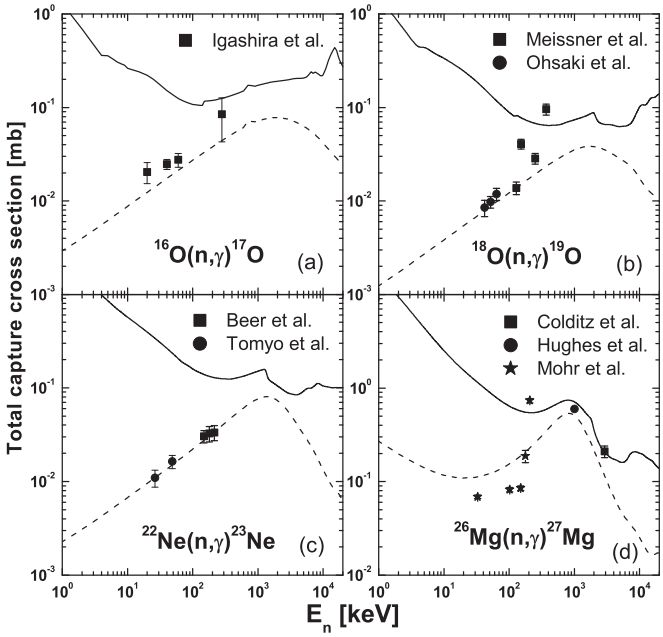

FIG. 2. Comparison of our calculated neutron-capture cross sections and the experimental data for four light nuclei. The solid lines correspond to the total (CNC + PEC + DIC) neutron-capture cross sections, while the dashed lines correspond to the DIC contribution only. Experimental data are taken from Ref. [53] for ^{16}O(n,γ)^{17}O, [54,55] for ^{18}O(n,γ)^{19}O, [56,57] for ^{22}Ne(n,γ)^{22}Ne, [58–60] for ^{26}Mg(n,γ)^{27}Mg.

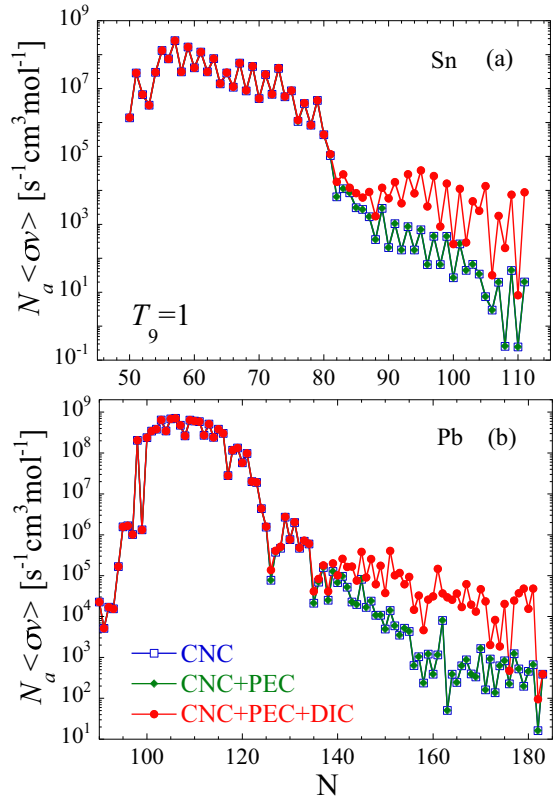

FIG. 3. (Color online) Total (CNC + PEC + DIC), CNC + PEC, and CNC reaction rates for (a) Sn and (b) Pb isotopic chains (from the proton to the neutron drip lines) at $T_9 = 1$ (T_9 denotes the temperature in 10^9 K).

charged-particle fusion reactions on light and medium-mass elements that play a role when the nuclear statistical equilibrium freezes out are- included in addition to radiative neutron captures and photodisintegrations. The reaction rates on light species are taken from the NETGEN library, which includes all the latest compilations of experimentally determined reaction rates [71]. Experimentally unknown reactions are estimated with the TALYS code including or not the DIC contribution. Fission and β decays are also included, i.e., neutron-induced fission, spontaneous fission, β-delayed fission, photofission, as well as β-delayed neutron emission. The β-decay processes are taken from the updated version of the Gross Theory [72] based on the HFB-21 Q values, whereas all fission processes are estimated on the basis of the HFB-14 fission path and the full calculation of the corresponding barrier penetration [73]. The fission fragment distribution is taken from the SPY model as described in Ref. [74].

In the first r-process ν-driven wind scenario, the adopted wind model corresponds to a subsonic breeze expansion with an entropy $S = 200$, electron fraction $Y_e = 0.41$, mass-loss rate $dM/dt = 6 \times 10^{-7} M_\odot$ s^{-1}, and breeze solution $f_w = 3$ (see Refs. [1,67] for more details). For such conditions, the expansion is rather fast, so that the neutron irradiation responsible for the r processing takes place at low temperature and the final abundance distribution is sensitive to the adopted neutron-capture rates, as shown in Fig. 7. Note that the total CNC + PEC + DIC case is compared here to the case where only the CNC mechanism is included, since this latter is the one that has been used in almost all existing r-process simulations up to now. For exotic neutron-rich nuclei, the PEC gives a relatively small contribution with respect to the CNC (see Fig. 3 and Ref. [3]) when compared to the impact of the DIC (Fig. 6). The major differences in the prediction are found around the $A \simeq 160$–170 rare-earth peak, where the inclusion of the DIC calculation gives rise to a smaller production. This effect can be attributed to the fast DIC rates in the vicinity of

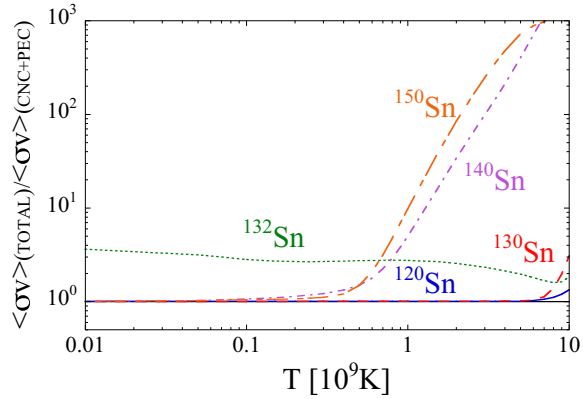

FIG. 4. (Color online) Ratio between the total (CNC + PEC + DIC) and CNC + PEC reaction rates for five Sn isotopes as a function of the temperature.

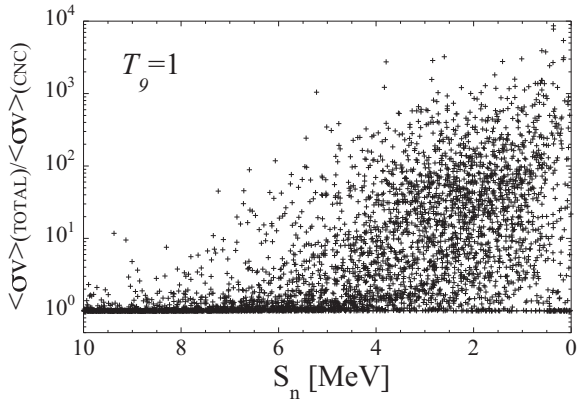

FIG. 5. Ratio between the total (CNC + PEC + DIC) and CNC reaction rates for all nuclei with $8 \leqslant Z \leqslant 92$ and lying between the $N = Z$ and the neutron drip line, as a function of the neutron-separation energy S_n.

the neutron-rich nuclei with $Z \simeq 55$ and $N \simeq 115$ (Fig. 6). The $N = 126$ peak is also found to be slightly different; the DIC contribution tends to move it to lower A values or, equivalently, to increase the production of the $A \gtrsim 195$ nuclei and decrease those of the $A \gtrsim 195$ species. These differences arise from the larger rates obtained in the $Z \simeq 70$ neutron-rich region (see Fig. 6) when including the DIC component.

In the second r-process scenario, we study the nucleosynthesis in the matter that is dynamically ejected by tidal and pressure forces during the merging of two binary neutron stars. Full details about the hydrodynamical simulations can be found in Refs. [69,70]. In this scenario, large neutron-to-seed ratios drive the nuclear flow into the very-heavy-mass region, leading to multiple fission recycling at relatively low temperatures. As a consequence, the resulting abundance distribution becomes independent of the initial conditions, but remains sensitive to the neutron-capture rates as shown in Fig. 8. The impact of the DIC component is seen to be rather similar to that found in the case of the subsonic

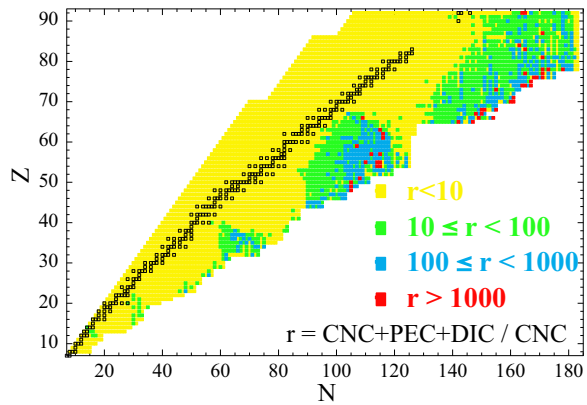

FIG. 6. (Color online) Representation in the (N, Z) plane of the ratio r between the total (CNC + PEC + DIC) and CNC reaction rates for all nuclei with $8 \leqslant Z \leqslant 92$ and lying between the $N = Z$ and neutron drip line.

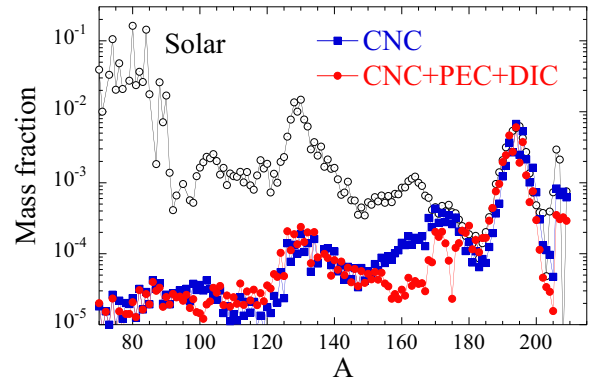

FIG. 7. (Color online) Distributions of the r-nuclide abundances obtained within the neutrino-driven wind corresponding to an entropy $S = 200$, electron fraction $Y_e = 0.41$, mass-loss rate $dM/dt = 6 \times 10^{-7} M_\odot$ s^{-1}, and breeze solution $f_w = 3$ (see Refs. [1,67] for more details). The distributions are compared with the solar r-abundance distribution (dotted circles).

wind, i.e., a small shift of the $N = 126$ peak to lower masses and the $A \simeq 160$–180 region affected by the capture of late neutrons [74]. These effects could have some impact when trying to reproduce the solar system abundances in this specific scenario.

VII. SUMMARY AND OUTLOOK

The three CNC, PEC, and DIC reaction mechanisms have been studied systematically and comprehensively within a unique and consistent framework obtained with the modern reaction code TALYS. Of particular relevance, the same nuclear inputs are used consistently to determine the three contributions; in particular, the same nucleon-nucleus optical potential ensures that the three components are calculated on the same footing and represents partial fluxes of the same total reaction cross section. The nuclear-structure ingredients of relevance, i.e., the nuclear mass, electromagnetic multipole moments, spectroscopic factor, γ-ray strength function, neutron-nucleus

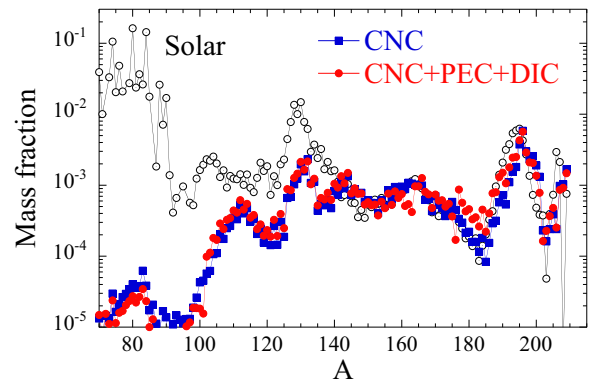

FIG. 8. (Color online) Final nuclear-abundance distributions of the ejecta from a 1.35–$1.35 M_\odot$ (squares) neutron star merger as functions of atomic mass. The distributions are normalized to the solar r-abundance distribution (dotted circles).

interaction potential, and excited-level scheme, are determined from experimental data whenever available and, if not, from global microscopic nuclear models (except for the spectroscopic factors for which an average value is adopted).

We have shown that the calculated neutron total capture cross sections including all three contributions are in fair agreement with experimental data for targets with mass number $A > 26$. For lighter nuclei, the experimental cross sections tend to be overestimated by the CNC contribution but can be rather well reproduced if only the DIC component is considered. The CNC reaction rate described by the Hauser–Feshbach model is known to be valid provided the number of levels available to the incident nucleon in the compound nucleus is large enough and their energy and width are randomly distributed within the contributing energy interval to ensure a continuum superposition of resonances. These conditions might not be fulfilled for light nuclei with mass number $A < 26$, so that special care should be taken when extrapolating the statistical predictions to these nuclei. One way to account for such an overestimate of the reaction rate is to bring a more detailed description of the CNC mechanism when only a few resonant states are available, e.g., within the Breit–Wigner approach.

When considering exotic neutron-rich nuclei, the DIC component is found to significantly dominate the other two contributions. The corresponding DIC is found to be two to three orders of magnitude larger than that obtained within the Hauser–Feshbach approach and classically used in nucleosynthesis applications. Since all r-process calculations have made use of neutron-capture rates evaluated within the statistical model of Hauser–Feshbach and have neglected the DIC component, we have performed r-process calculations and compared the abundance predictions describing a subsonic neutrino-driven wind and the merging of two binary neutron stars. For r processes taking place in a cold environment, we find that the impact on $170 \leqslant A \leqslant 200$ abundances can be significant. However, further improvements of the nuclear ingredients required for a proper description of the DIC cross section for exotic neutron-rich nuclei are needed.

ACKNOWLEDGMENTS

This work has been supported by the Communauté Française de Belgique (Actions de Recherche Concertées). Y.X. and S.G acknowledge the support of the F.R.S.-FNRS.

[1] M. Arnould, S. Goriely, and K. Takahashi, Phys. Rep. **450**, 97 (2007).
[2] W. Hauser and H. Feshbach, Phys. Rev. **87**, 366 (1952).
[3] S. Goriely, S. Hilaire, and A. J. Koning, Astron. Astrophys. **487**, 767 (2008).
[4] G. R. Satchler, *Introduction to Nuclear Reactions* (Macmillan Press Ltd., London, 1980).
[5] J. E. Lynn, *The Theory of Neutron Resonance Reactions* (Clarendon Press, Oxford, 1968).
[6] C. Rolfs, Nucl. Phys. A **217**, 29 (1973).
[7] S. Goriely, Astron. Astrophys. **325**, 414 (1997).
[8] P. Descouvemont, J. Phys. G **35**, 014006 (2008).
[9] Y. Xu and S. Goriely, Phys. Rev. C **86**, 045801 (2012).
[10] H. Oberhummer and G. Staudt, in *Nuclei in the Cosmos*, edited by H. Oberhummer (Springer Verlag, Heidelberg, 1991), p. 29.
[11] Y. Xu, K. Takahashi, S. Goriely, M. Arnould, M. Ohta, and H. Utsunomiya, Nucl. Phys. A **918**, 61 (2013).
[12] A. Mengoni, T. Otsuka, and M. Ishihara, Phys. Rev. C **52**, R2334 (1995).
[13] H. Beer, C. Coceva, P. V. Sedyshev, Y. P. Popov, H. Herndl, R. Hofinger, P. Mohr, and H. Oberhummer, Phys. Rev. C **54**, 2014 (1996).
[14] S. Chiba, H. Koura, T. Hayakawa, T. Maruyama, T. Kawano, and T. Kajino, Phys. Rev. C **77**, 015809 (2008).
[15] J. T. Huang, C. A. Berutulani, and V. Guimaraes, At. Data Nucl. Data Tables **96**, 828 (2010).
[16] A. J. Koning and M. C. Duijvestijn, Nucl. Phys. A **744**, 15 (2004).
[17] A. J. Koning, S. Hilaire, and M. C. Duijvestijn, NRG-report 21297/04.62741/P (2004). Also available at http://www.talys.eu
[18] A. J. Koning, S. Hilaire, and M. Duijvestijn, *Nuclear Data for Science and Technology*, edited by O. Bersillon *et al.* (EDP Sciences, Paris, 2008), p. 211.
[19] A. J. Koning and D. Rochman, Nucl. Data Sheets **113**, 2841 (2012).
[20] S. Hilaire, C. Lagrange, and A. J. Koning, Ann. Phys. (NY) **306**, 209 (2003).
[21] G. Audi, M. Wang, A. H. Wapstra, F. G. Kondev, M. MacCormick, X. Xu, and B. Pfeiffer, Chin. Phys. C **36**, 1287 (2012).
[22] S. Goriely, N. Chamel, and J. M. Pearson, Phys. Rev. C **82**, 035804 (2010).
[23] P. Raghavan, At. Data Nucl. Data Tables **42**, 189 (1989).
[24] Y. Xu, S. Goriely, A. Jorissen, G. L. Chen, and M. Arnould, Astron. Astrophys. **549**, A106 (2013).
[25] S. Goriely, Phys. Lett. B **436**, 10 (1998).
[26] S. Goriely, E. Khan, and M. Samyn, Nucl. Phys. A **739**, 331 (2004).
[27] E. Khan *et al.*, Nucl. Phys. A **694**, 103 (2001).
[28] E. Bauge, J. P. Delaroche, and M. Girod, Phys. Rev. C **63**, 024607 (2001).
[29] J. P. Jeukenne, A. Lejeune, and C. Mahaux, Phys. Rev. C **16**, 80 (1977).
[30] E. Bauge, J. P. Delaroche, M. Girod, G. Haouat, J. Lachkar, Y. Patin, J. Sigaud, and J. Chardine, Phys. Rev. C **61**, 034306 (2000).
[31] H. Scheit, F. Maréchal, T. Glasmacher, E. Bauge, Y. Blumenfeld, J. P. Delaroche, M. Girod, R. W. Ibbotson, K. W. Kemper, J. Libert, B. Pritychenko, and T. Suomijärvi, Phys. Rev. C **63**, 014604 (2000).
[32] E. Bauge, J. P. Delaroche, and M. Girod, Phys. Rev. C **58**, 1118 (1998).
[33] J. P. Jeukenne, A. Lejeune, and C. Mahaux, Phys. Rev. C **10**, 1391 (1974).
[34] K. H. Guber, L. C. Leal, R. O. Sayer, R. R. Spencer, P. E. Koehler, T. E. Valentine, H. Derrien, and J. A. Harvey, J. Nucl. Sci. Technol. Suppl. **2**, 346 (2002).

[35] G. Calvi, R. Potenza, R. Ricamo, and D. Vinciguerra, Nucl. Phys. **39**, 621 (1962).
[36] R. L. Henkel and H. H. Barschall, Phys. Rev. **80**, 145 (1950).
[37] A. G. Dovbenko, V. E. Kolesov, V. P. Koroleva, and V. A. Tolstikov, Atomnaya Energiya **23**, 151 (1967).
[38] A. Tomyo, Y. Temma, M. Segawa, Y. Nagai, T. Shima, H. Makii, M. Igashira, T. Ohsaki, T. Masaki, and J. Nishiyama, Astrophys. J. **623**, 153 (2005).
[39] A. R. De L. Musgrove, B. J. Allen, J. W. Boldeman, R. L. Macklin, and R. R. Winters, Nucl. Phys. A **270**, 108 (1976).
[40] S. P. Kapchigashev and Yu. P. Popov, *Proc. of Neutron Interactions Conference, Dubna* (JINR, Dubna, Russia, 1964), p. 104.
[41] V. A. Tolstikov, V. P. Koroleva, V. E. Kolesov, A. G. Dovbenko, and Yu. N. Shubin, Atomnaya Energiya **24**, 576 (1968).
[42] V. M. Timokhov, M. V. Bokhovko, M. V. Isakov, L. E. Kazakov, V. N. Kononov, G. N. Manturov, E. D. Poletaev, and V. G. Pronyaev, Obninsk Reports No. 1921, Fiz.-Energ Institut (1988).
[43] H. Beer, G. Walter, R. L. Macklin, and P. J. Patchett, Phys. Rev. C **30**, 464 (1984).
[44] R. L. Macklin and J. H. Gibbons, Phys. Rev. **159**, 1007 (1967).
[45] K. Wisshak, F. Voss, F. Kappeler, and L. Kazakov, Phys. Rev. C **73**, 015807 (2006).
[46] H. Beer, W. Rochow, F. Kappeler, and T. Rauscher, Nucl. Phys. A **718**, 518 (2003).
[47] I. Bergqvist, D. M. Drake, and D. K. McDaniels, Nucl. Phys. A **191**, 641 (1972).
[48] G. Aerts *et al.* (n-TOF collaboration), Phys. Rev. C **73**, 054610 (2006).
[49] W. Y. Baek, G. N. Kim, M. H. Cho, I. S. Ko, W. Namkung, Yu. V. Grigoriev, H. Faikov-Stanczyk, V. N. Shvetshov, and W. I. Furman, Nucl. Instrum. Methods Phys. Res., Sect. B **168**, 453 (2000).
[50] R. E. Chrien, H. I. Liou, M. J. Kenny, and M. L. Stelts, Nucl. Sci. Eng. **72**, 202 (1979).
[51] D. Karamanis *et al.*, Nucl. Sci. Eng. **139**, 282 (2001).
[52] H. Naik *et al.*, Eur. Phys. J. A **47**, 51 (2011).
[53] M. Igashira, Y. Nagai, K. Masuda, T. Ohsaki, and H. Kitazawa, Astrophys. J. **441**, 89 (1995).
[54] J. Meissner, H. Schatz, J. Gorres, H. Herndl, M. Wiescher, H. Beer, and F. Kappeler, Phys. Rev. C **53**, 459 (1996).
[55] T. Ohsaki, M. Igashira, Y. Nagai, M. Segawa, and K. Muto, Phys. Rev. C **77**, 051303 (2008).
[56] H. Beer, P. V. Sedyshev, W. Rochow, P. Mohr, and H. Oberhummer, Nucl. Phys. A **705**, 239 (2002).
[57] A. Tomyo, Y. Nagai, Y. Nobuhara, T. Shima, H. Makii, K. Mishima, and M. Igashira, Nucl. Phys. A **718**, 527 (2003).
[58] J. Colditz and P. Hille, Oesterr. Akad. Wiss., Math-Naturw. Kl., Anzeiger **105**, 236 (1968).
[59] D. J. Hughes, R. C. Garth, and J. S. Levin, Phys. Rev. **91**, 1423 (1953).
[60] P. Mohr, H. Beer, H. Oberhummer, and G. Staudt, Phys. Rev. C **58**, 932 (1998).
[61] S. Goriely, S. Hilaire, and A. J. Koning, Phys. Rev. C **78**, 064307 (2008).
[62] G. R. Satchler, *Direct Nuclear Reactions* (Clarendon Press, Oxford, 1983).
[63] H. Oberhummer, W. Balogh, R. Bieber, H. Herndl, U. Langer, T. Rauscher, and H. Beer, in *International Conference on Exotic Nuclei and Atomic Masses*, edited by M. de Saint Simon and O. Sorlin (Editions Frontières, Gif-sur-Yvette, France, 1995), p. 649.
[64] R. Capote *et al.*, Nucl. Data Sheets **110**, 3107 (2009).
[65] C. Sneden, J. J. Cowan, and R. Gallino, Annu. Rev. Astron. Astrophys. **46**, 241 (2008).
[66] K. Takahashi, J. Witti, and T.-T. Janka, Astron. Astrophys. **286**, 857 (1994).
[67] K. Takahashi and H.-T. Janka, in *Origin of Matter and Evolution of Galaxies*, edited by T. Kajino, S. Kubono, and Y. Yoshii (World Scientific, Singapore, 1997), p. 213.
[68] S. Wanajo, H.-T. Janka, and B. Müller., Astrophys. J. Lett. **726**, L15 (2011).
[69] S. Goriely, A. Bauswein, and H.-T. Janka, Astrophys. J. Lett. **738**, L32 (2011).
[70] A. Bauswein, S. Goriely, and H.-T. Janka, Astrophys. J. **773**, 78 (2013).
[71] Y. Xu, S. Goriely, A. Jorissen, G. L. Chen, and M. Arnould, Astron. Astrophys. **549**, A106 (2013).
[72] T. Tachibana, M. Yamada, and Y. Yoshida, Prog. Theor. Phys. **84**, 641 (1990).
[73] S. Goriely, S. Hilaire, A. J. Koning, M. Sin, and R. Capote, Phys. Rev. C **79**, 024612 (2009).
[74] S. Goriely, J.-L. Sida, J.-F. Lemaître, S. Panebianco, N. Dubray, S. Hilaire, A. Bauswein, and H.-T. Janka, Phys. Rev. Lett. **111**, 242502 (2013).